Chapter 4
Attenuation Compensation and Estimation

Timothy A. Bigelow and Yassin Labyed

Abstract Estimating the losses of ultrasound signal energy with propagation depth as a function of frequency is essential for quantifying tissue properties. Specifically, ultrasound attenuation is used to correct for spectral distortion prior to estimating quantitative ultrasound parameters to assess the tissue. Ultrasound attenuation can also be used independently to characterize the tissue. In this chapter, we review the primary algorithms for estimating both the local attenuation within a region of interest as well as the total attenuation between a region of interest and an ultrasound source. The strengths and weaknesses of each algorithm are also discussed.

Keywords Attenuation · Local attenuation · Total attenuation · Spectral difference method · Spectral-log difference method · Hybrid method · Spectral-fit method · Multiple filter method

4.1 Introduction

When attempting to characterize tissue based on the frequency spectrum of backscattered ultrasound echoes, it is critically important to correctly compensate for attenuation. Because both scattering and attenuation impact the frequency spectrum, the effects of attenuation must be removed before the scattering properties can be extracted for diagnostic purposes. For the purpose of tissue characterization, there are two different attenuation parameters to be considered. First, there is the **local attenuation**. The local attenuation is the attenuation within a

T. A. Bigelow (✉)
Iowa State University, 2113 Coover Hall, Ames, IA 50011, USA
e-mail: bigelow@iastate.edu

Y. Labyed
Los Alamos National Lab, Los Alamos, NM, USA

J. Mamou and M. L. Oelze (eds.), *Quantitative Ultrasound in Soft Tissues*, DOI: 10.1007/978-94-007-6952-6_4,

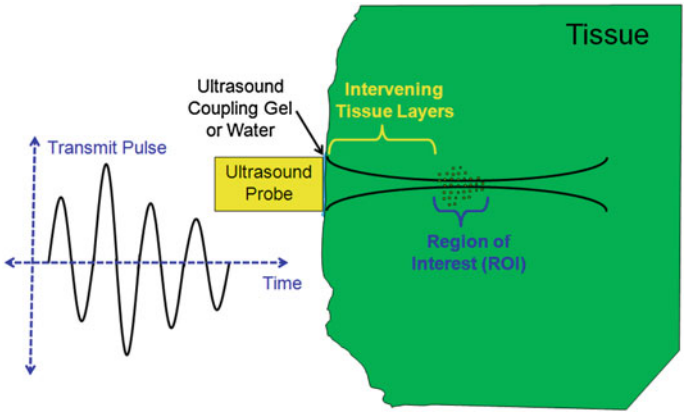

Fig. 4.1 Illustration of tissue when performing ultrasound tissue characterization

region of interest and is used primarily to quantify the tissue properties of that region. It can also be used to improve the accuracy of scatterer property estimates, e.g., scatterer size and acoustic concentration, as will be discussed in more detail later in this chapter. The second and most important type of **attenuation is the total attenuation**. The total attenuation is the effective attenuation along the propagation path from the source thru the intervening tissue layers to the region of interest. Figure 4.1 shows an image of the different regions corresponding to the local and total attenuation. It is more difficult to obtain accurate estimates of the backscatter coefficient and corresponding scatterer property estimates derived from the backscatter coefficient without an accurate estimate for the total attenuation. In this chapter, we will review how the attenuation impacts the backscattered power spectrum as well as summarize the basic algorithms that have been developed to estimate both total and local attenuation.

4.2 Impact of Attenuation on Backscattered Power Spectrum

Before discussing the various algorithms that have been developed to estimate the total and local attenuation, we will briefly review how these attenuation parameters relate to the backscattered power spectrum. The backscattered power spectrum from a region of interest in an unknown sample is given by Bigelow (2004) and Bigelow and O'Brien (2004a, b)

$$S_s(f) \propto \left[\begin{array}{c} f^4 |H(f)|^4 |V_{inc}(f)|^2 \exp(-4\alpha_{tot}(f) z_T) \\ \times M_\gamma \cdot F_\gamma(f, a_{eff}) D(f, \alpha_{loc}) \end{array} \right] \tag{4.1}$$

In this equation, f is frequency, $H(f)$ is the dimensionless filtering characteristics of the ultrasound source, $|V_{inc}(f)|$ is the power spectrum of the voltage pulse applied to the ultrasound source, and z_T is the distance from the ultrasound source to the beginning of the region of interest in the tissue. The term $\alpha_{tot}(f)$ is the total attenuation along the propagation path, as was described previously, and is given by

$$\alpha_{tot}(f) = \left(\sum_{j=1}^{N-1} \alpha_j(f) \frac{\Delta z_j}{z_T} \right) \tag{4.2}$$

where α_j is the attenuation in each of the intervening tissue layers of thickness Δz_j. Also, $F_\gamma\left(f, a_{eff}\right)$ is the form factor which captures the frequency dependence of the scattering while M_γ is the acoustic concentration (Insana et al. 1990). Typical form factors for tissue and tissue-mimicking phantoms include the Gaussian form factor, the fluid-filled sphere form factor, and the spherical-shell form factor.

$$\begin{aligned} F_{\gamma\_Gaussian}\left(f,\ a_{eff}\right) &= \exp\left(-0.827\left(k \cdot a_{eff}\right)\right) \\ F_{\gamma\_Sphere}\left(f,\ a_{eff}\right) &= \left[\frac{j_1\left(2k \cdot a_{eff}\right)}{(2/3)k \cdot a_{eff}}\right]^2 \\ F_{\gamma\_Shell}\left(f,\ a_{eff}\right) &= \left[j_o\left(2k \cdot a_{eff}\right)\right]^2 \end{aligned} \tag{4.3}$$

The development of more complicated form factors to accurately model tissue is the subject of current study (Oelze and O'Brien 2006).

The remaining term from Eq. (4.1), $D(f, \alpha_{loc})$ takes into account both the diffraction of the acoustic waves (i.e., focusing) and the local attenuation, $\alpha_{loc}(f)$ of the tissue in the region of interest and is given by

$$\begin{aligned} D(f, \alpha_{loc}) = &\exp(-4\alpha_{loc}(f) z_o) \\ &\times \int_{-L/2}^{L/2} \left[g_{win}(s_z) \exp(-4\alpha_{loc}(f) s_z) D_{focus}(f, s_z) \right] ds_z \end{aligned} \tag{4.4}$$

where the variable of integration, s_z, increases as we move away from the source. In this equation, g_{win} is the windowing function used to gate the backscattered echoes when selecting an analysis region. Common windowing functions include rectangular, Hamming, and Hanning windows. Also, L is the length of the windowing function expressed as a distance and z_o is the distance from the beginning of the region of interest (ROI) to the center of the current windowed analysis region within the ROI. We distinguish here between the larger ROI, or the region over which the attenuation estimate is obtained, and the smaller windowed analysis region, or the region where the power spectrum is estimated. The attenuation estimation algorithms require finding multiple power spectra from different analysis regions within the ROI in order to find the attenuation of the ROI. The windowed analysis region is illustrated in Fig. 4.2.

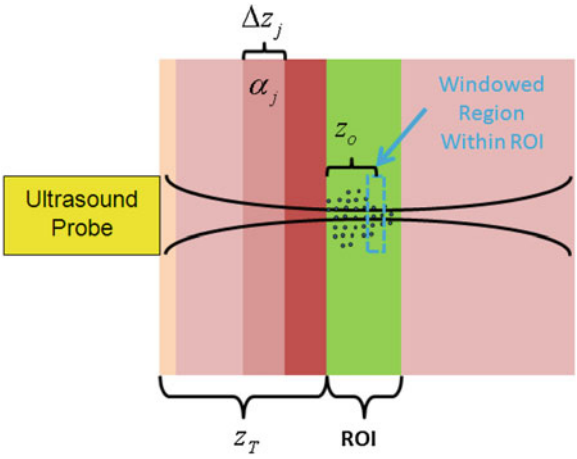

Fig. 4.2 Illustration showing coordinates when defining variables in backscattered power spectrum

The term within the integral $D_{focus}(f, s_z)$ takes into account focusing and is given by

$$D_{focus}(f, s_z) = \left[\begin{array}{c} \exp\left(\frac{-2((z_T+z_o-F_{transmit})+s_z)^2}{(w_{z\_transmit}(f))^2}\right) \\ \times \exp\left(\frac{-2((z_T+z_o-F_{rcv})+s_z)^2}{(w_{z\_rcv}(f))^2}\right) \end{array} \right] \tag{4.5}$$

assuming the beam profile on transmit and receive can be approximated by a Gaussian function; an approximation that is reasonable for most sources (Barber 1991; Bigelow 2004; Bigelow and O'Brien 2004a, b). In this equation, $F_{transmit}$ and F_{rcv} are the distance from the aperture plane to the transmit and receive foci respectively. Also, $w_{z\_transmit}(f)$ and $w_{z\_rcv}(f)$ are the effective Gaussian depths of focus for the transmit and receive foci, respectively. For a spherically focused source, w_z is approximately equal to $6.01\lambda(\text{f\#})^2$ where λ is the wavelength and f# is the f-number for the source.

From Eq. (4.4), it is clear that the impact of local attenuation on the backscattered power spectrum is coupled with the diffraction of the acoustic field via the integral expression. This coupling can make the assessment of backscatter more challenging. As a result, various investigators have attempted to isolate the local attenuation and focusing effects on the spectrum so that each can be corrected independently. The most common approach, termed **point compensation**, assumes that the size of the windowing function is so small that g_{win} can be approximated by an impulse function (Oelze and O'Brien 2002; Bigelow 2004; Bigelow and O'Brien 2004a, b). Under this approximation, Eq. (4.4) becomes

$$D(f, \alpha_{loc}) = \exp(-4\alpha_{loc}(f)z_o)\left[\begin{array}{c} \exp\left(\frac{-2(z_T+z_o-F_{transmit})^2}{(w_{z\_transmit}(f))^2}\right) \\ \times \exp\left(\frac{-2(z_T+z_o-F_{rcv})^2}{(w_{z\_rcv}(f))^2}\right) \end{array} \right] \tag{4.6}$$

where the local attenuation term and diffraction terms have been decoupled.

Another approach to decouple the local attenuation and diffraction is to use an approximate value for the local attenuation within the integral (Bigelow and O'Brien 2006). This approach is used in all tissue characterization methods that divide the power spectrum from the sample by the power spectrum from a reference phantom as will be discussed in more detail later in the chapter. Under this approximation Eq. (4.4) becomes

$$D(f,\alpha_{loc}) = \exp(-4\alpha_{loc}(f)z_o) \times \int_{-L/2}^{L/2} \left[g_{win}(s_z)\exp\left(-4\alpha_{approximate}(f)s_z\right)D_{focus}(f,s_z)\right]ds_z \tag{4.7}$$

The optimal choice for $\alpha_{approximate}(f)$ was shown to be given by

$$\alpha_{approximate}(f) \cong \sqrt{\frac{\alpha_{high}^2(f)+\alpha_{low}^2(f)}{2}} \tag{4.8}$$

where $\alpha_{high}(f)$ and $\alpha_{low}(f)$ are the largest and smallest attenuation values expected in the tissue region (Bigelow and O'Brien 2006).

4.3 Local Attenuation Estimation Algorithms

Now that we have reviewed how local and total attenuation impacts the backscattered power spectrum, we can review some of the algorithms used to estimate the attenuation within a region of interest. While this local attenuation can be used to improve the estimate of the scattering properties for the tissue, it is typically used independently to characterize the tissue for diagnostic purposes. We will focus on four of the most common local attenuation estimation algorithms.

4.3.1 Spectral Shift Algorithm for Local Attenuation Estimation

One of the most common algorithms for estimating the attenuation within a region of interest is the spectral-shift algorithm. This algorithm uses the down shift in center frequency of the power spectrum versus propagation depth to estimate the attenuation slope, α_0, where the local attenuation is assumed to have the form $\alpha_{loc}(f) = \alpha_0 f + \beta_b$ (Narayana and Ophir 1983a, b; Oosterveld et al. 1991; Baldeweck et al. 1993, 1994, 1995; Girault et al. 1998; Kim and Varghese 2007). This algorithm has been implemented in both the frequency and the time domain, where the time-domain implementation requires utilizing an autoregressive

approach (Baldeweck et al. 1993, 1994, 1995; Girault et al. 1998). We will derive the algorithm in the frequency domain because focusing has not been accounted for in the autoregressive approach.

The spectral shift algorithm begins by assuming that the backscattered power spectrum can be approximated by a Gaussian function. As a result, Eq. (4.1) can be written as

$$S_s(f) \propto \exp\left(-\frac{(f-f_o)^2}{2\sigma_\omega^2}\right) D(f,\ \alpha_{loc}). \tag{4.9}$$

Traditionally, the spectral-shift algorithm has been implemented assuming weakly-focused sources where diffraction effects in the ROI can be neglected. In addition, small windows are typically used resulting in the assumption that point compensation is valid. Hence, Eq. (4.9) can be written as

$$S_s(f) \propto \exp\left(-\frac{(f-f_o)^2}{2\sigma_\omega^2}\right) \exp(-4\alpha_o \cdot f z_o). \tag{4.10}$$

However, multiplying the Gaussian function by the decaying exponential is just a Gaussian transformation resulting in a new Gaussian function.

$$S_s(f) \propto \exp\left(-\frac{\left(f-\tilde{f}_o(z_o)\right)^2}{2\sigma_\omega^2}\right) \tag{4.11}$$

where

$$\tilde{f}_o(z_o) = f_o - 4\sigma_\omega^2 \alpha_o \cdot z_o. \tag{4.12}$$

Therefore, the attenuation slope can be found by selecting multiple windows within a ROI (i.e., different z_o). The power spectrum for each window is then calculated and fit by a Gaussian function to find the center frequency, $\tilde{f}_o$, and bandwidth, σ_ω^2. The attenuation slope can then be calculated from the change in center frequency with depth,

$$\alpha_o = -\frac{1}{4\sigma_\omega^2}\frac{\partial \tilde{f}_o}{\partial z_o}. \tag{4.13}$$

Importance of Finding the Usable Frequency Range: When fitting a function to a spectrum it is critically important to perform the fit only with values from the spectrum that are not dominated by noise. Therefore, the first step in any frequency domain algorithm is to first find the usable frequency range from the power spectrum. One can do this from either a visible inspection of the spectrum or using a computer program that identifies the noise floor for the spectral data and always operates above this noise floor.

Hint on Finding Center Frequency and Bandwidth: When finding the center frequency and bandwidth from a fit to a Gaussian function, we have found that a more accurate fit can be obtained by performing the fit in the log domain. Therefore, we find the values of $\tilde{f}_o$ and σ_ω^2 that minimize the function in Eq. (4.14).

$$mse = \underset{f}{\text{mean}}\left[\left(\begin{array}{l}\log\left(e^{\left(-\frac{(f-\tilde{f}_o)^2}{2\sigma_\omega^2}\right)}\right) - \log\left(\frac{S_s(f)}{\max\limits_f(S_s(f))}\right) \\ -\underset{f}{\text{mean}}\left(\log\left(e^{\left(-\frac{(f-\tilde{f}_o)^2}{2\sigma_\omega^2}\right)}\right) - \log\left(\frac{S_s(f)}{\max\limits_f(S_s(f))}\right)\right)\end{array}\right)^2\right]. \quad (4.14)$$

The expression derived in Eq. (4.13) is valid only when diffraction effects can be neglected (Bigelow et al. 2008; Kim and Varghese 2008). Otherwise, a correction needs to be applied as indicated in Fig. 4.3 taken from Bigelow et al. (2008).

From this figure, it is clear that without focusing compensation, ROIs before the focus underestimate the attenuation slope while ROIs beyond the focus overestimate the attenuation slope. When the windowed regions is close to the focus, we use the following correction

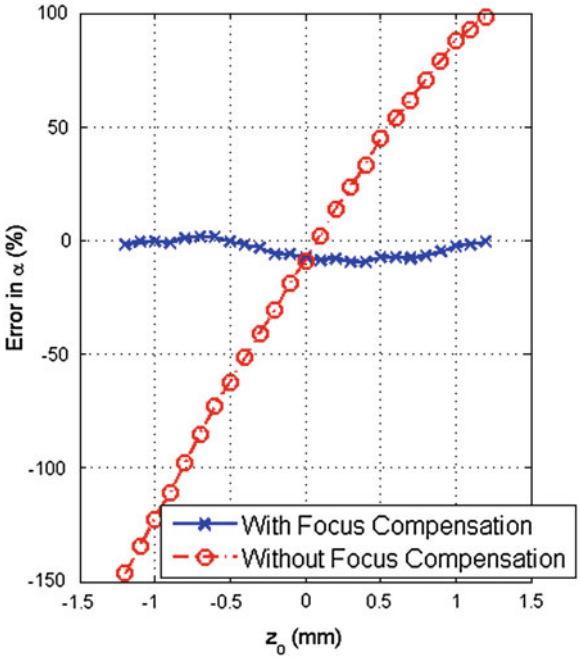

Fig. 4.3 Error in attenuation estimate both with and without focusing compensation for a simulated 33 MHz spherically focused transducer intended to assess cervical ripening in rats taken from Bigelow et al. (2008). The source had a focal length 9 mm and $z_o = 0$ in this figure corresponds to the focus

$$\left[\exp\left(\frac{2(z_T + z_o - F_{transmit})^2}{(w_{z\_transmit}(f))^2}\right) \cdot \exp\left(\frac{2(z_T + z_o - F_{rcv})^2}{(w_{z\_rcv}(f))^2}\right)\right] \tag{4.15}$$

before finding the center frequency. This correction is based on the assumption that the beam can be approximated by a Gaussian function in the focal region (Bigelow et al. 2008).

4.3.2 Spectral Difference Method for Local Attenuation Estimation

Another common algorithm for estimating the local attenuation from an ROI is the spectral difference method (Parker and Waag 1983; Parker et al. 1988; Yao et al. 1990). The spectral difference method is sometimes referred to as the reference-phantom method because it uses a well-characterized reference phantom to correct for diffraction effects. In the spectral difference method, multiple overlapping windows are positioned throughout the ROI as shown in Fig. 4.4. An overlap of 50 % between adjacent windows is common; however, other overlap values have been used. Power spectra from corresponding windows in a reference phantom are also acquired.

Importance of Sound Speed: It is important to use a tissue-mimicking phantom with a sound speed similar to the expected sound speed of the tissue so that the diffraction properties are similar when estimating the attenuation.

After obtaining the power spectrum from each window for the sample and the reference, the power spectra are divided to give

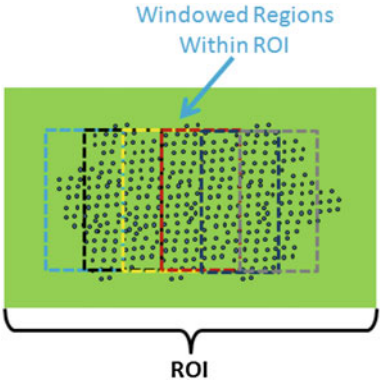

Fig. 4.4 Illustration of windowed regions within ROI when implementing the spectral difference algorithm

$$\frac{S_s(f)}{S_{ref}(f)} \propto \left[\frac{\exp(-4\alpha_{tot}(f)z_T) \cdot M_\gamma F_\gamma(f) D(f,\, \alpha_{loc})}{\exp\left(-4\alpha_{ref}(f)z_T\right) \cdot M_{\gamma\_ref} F_{\gamma\_ref}(f) D\left(f,\, \alpha_{ref}\right)} \right] \tag{4.16}$$

where $\alpha_{ref}(f)$ is the attenuation of the reference phantom and $F_{\gamma\_ref}(f)$ is the form factor describing the frequency dependence of the scattering from the phantom. Using the approximation in Eqs. (4.7) and (4.16) simplifies to

$$\frac{S_s(f)}{S_{ref}(f)} \propto \left[\begin{matrix} \exp\left(-4\left(\alpha_{tot}(f) - \alpha_{ref}(f)\right)z_T\right) \\ \exp\left(-4\left(\alpha_{loc}(f) - \alpha_{ref}(f)\right)z_o\right) \frac{M_\gamma F_\gamma(f)}{M_{\gamma\_ref} F_{\gamma\_ref}(f)} \end{matrix} \right]. \tag{4.17}$$

Taking the natural logarithm of the above relation gives,

$$S(f) = \ln\left(\frac{S_s(f)}{S_{ref}(f)}\right) = 4\left(\alpha_{ref}(f) - \alpha_{loc}(f)\right)z_o + C(f) \tag{4.18}$$

where $C(f)$ is a function of frequency that depends on the scattering properties and total attenuation of the sample and reference phantoms. $C(f)$ does not depend on z_o provided the ROI is homogeneous. The attenuation of the sample is calculated from the change in $S(f)$ with z_o, i.e.,

$$\alpha_{loc}(f) = \alpha_{ref}(f) - \frac{1}{4}\frac{\partial S(f)}{\partial z_o}. \tag{4.19}$$

Importance of Homogeneous Region: The spectral difference method cannot be used to estimate the attenuation when the scattering properties change within the ROI as this would make $C(f)$ also a function of z_o (Labyed and Bigelow 2011).

4.3.3 Spectral Log Difference Method for Local Attenuation Estimation

A slightly modified form of the spectral-difference method is the spectral-log-difference method (Kuc and Schwartz 1979; Kuc 1980, 1984; Insana et al. 1983). This method is slightly less dependent on changes in the scattering properties of the medium (Labyed and Bigelow 2011). The method begins by finding the backscattered power spectrum from two windowed regions within an ROI; one at the proximal edge of the ROI, z_{op}, and one at the distal edge of the ROI, z_{od}, as shown in Fig. 4.5. Once again the power spectra from the windowed regions of the sample are divided by corresponding spectra from a reference phantom yielding

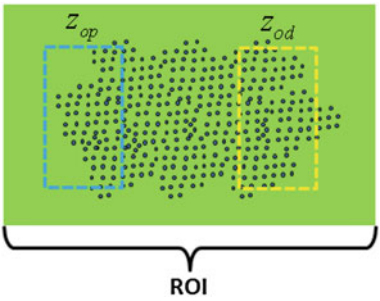

Fig. 4.5 Illustration of windowed regions within ROI when implementing the spectral log difference algorithm

$$S_p(f) = \ln\left(\frac{S_s(f, z_{op})}{S_{ref}(f, z_{op})}\right) = 4\left(\alpha_{ref}(f) - \alpha_{loc}(f)\right)z_{op} + C\left(f, z_{op}\right) \tag{4.20}$$

$$S_d(f) = \ln\left(\frac{S_s(f, z_{od})}{S_{ref}(f, z_{od})}\right) = 4\left(\alpha_{ref}(f) - \alpha_{loc}(f)\right)z_{od} + C(f, z_{od}) \tag{4.21}$$

where the subscript p refers to the proximal windowed region and the subscript d refers to the distal windowed region. Subtracting Eqs. (4.20) and (4.21) yields

$$S_\Delta(f) = S_p(f) - S_d(f) = \begin{bmatrix} 4\left(\alpha_{ref}(f) - \alpha_{loc}(f)\right)\left(z_{op} - z_{od}\right) \\ + C\left(f, z_{op}\right) - C(f, z_{od}) \end{bmatrix}. \tag{4.22}$$

Also, if we assume that the frequency dependence of the scattering does not change within the ROI for the sample (only possibly the acoustic concentration), then

$$C\left(f, z_{op}\right) - C(f, z_{od}) \cong C_\Delta\left(z_{op}, z_{od}\right) \tag{4.23}$$

which is independent of frequency (Labyed and Bigelow 2011). Therefore, the local attenuation within the ROI can be estimated by finding

$$\left[\frac{S_\Delta(f)}{4\left(z_{od} - z_{op}\right)} + \alpha_{ref}(f)\right] = \alpha_{loc}(f) + \frac{C_\Delta\left(z_{op}, z_{od}\right)}{4\left(z_{od} - z_{op}\right)} \tag{4.24}$$

and then performing a fit as a function of frequency to eliminate the C_Δ term. The most common approach is to assume a frequency dependence of $\alpha_{loc}(f) = \alpha_0 f + \beta_b$, and then perform a linear fit as a function of frequency to determine α_0.

ROI Size needed for Spectral Log Difference Method: A good rule of thumb is to have $(z_{od} \_ z_{op}) > 15$ pulse lengths and at least 15 independent echoes when using a linear approximation for the attenuation with the spectral-log-difference method. Smaller values tend to produce large variance of the estimates. However, these values are also dependent on the frequency range available for obtaining the estimates.

4.3.4 Hybrid Method for Local Attenuation Estimation

A third method for estimating the attenuation within an ROI is the hybrid method (Kim and Varghese 2008). The hybrid method has very similar performance to the spectral log-difference method (Labyed and Bigelow 2011). The hybrid method once again begins by calculating the power spectra for multiple windowed regions within an ROI and a corresponding reference phantom. The sample and reference power spectra are then divided yielding

$$\frac{S_s(f,z_o)}{S_{ref}(f,z_o)} \propto \begin{bmatrix} \exp\left(-4\left(\alpha_{tot}(f)-\alpha_{ref}(f)\right)z_T\right) \\ \exp\left(-4\left(\alpha_{loc}(f)-\alpha_{ref}(f)\right)z_o\right)\frac{M_\gamma(z_o)F_\gamma(f)}{M_{\gamma\_ref}(z_o)F_{\gamma\_ref}(f)} \end{bmatrix} \tag{4.25}$$

where once again we have assumed that the frequency dependence of the scattering **does not change** within the ROI. Note that a change in the acoustic concentration $M_\gamma(z_o)$ within the ROI does not impact the attenuation estimate. The power-spectra ratio for each window is then multiplied by a Gaussian function and corrected for the attenuation of the reference phantom to yield

$$\begin{aligned} GRS(f,\,z_o) &= \exp\left(-\frac{(f-f_c)^2}{2\sigma_c^2}\right)\frac{S_s(f,\,z_o)}{S_{ref}(f,\,z_o)}\exp\left(-4\alpha_{ref}(f)z_o\right) \\ &\propto \begin{bmatrix} \exp\left(-\dfrac{(f-f_c)^2}{2\sigma_c^2}\right)\exp\left(-4\left(\alpha_{tot}(f)-\alpha_{ref}(f)\right)z_T\right) \\ \exp(-4\alpha_{loc}(f)z_o)\dfrac{M_\gamma(z_o)F_\gamma(f)}{M_{\gamma\_ref}(z_o)F_{\gamma\_ref}(f)} \end{bmatrix} \end{aligned} \tag{4.26}$$

which is approximately equal to

$$GRS(f,\,z_o) \propto \left[\exp\left(-\frac{\left(f-\tilde{f}_c\right)^2}{2\tilde{\sigma}_c^2}\right)\exp(-4\alpha_{loc}(f)z_o)\right] \tag{4.27}$$

because of the frequency dependence of total attenuation and scattering. If we assume that the attenuation within the ROI has the form $\alpha_{loc}(f) = \alpha_0 f + \beta_b$, then Eq. (4.27) becomes

$$GRS(f,z_o) \propto e^{-\frac{(f-\tilde{f}_c)^2}{2\tilde{\sigma}_c^2}}e^{-4\alpha_o f z_o} \propto \exp\left(-\frac{\left(f-\tilde{f}_c'(z_o)\right)^2}{2\tilde{\sigma}_c^2}\right) \tag{4.28}$$

where

$$\tilde{f}_c'(z_o) = \tilde{f}_c - 4\tilde{\sigma}_c^2\alpha_o \cdot z_o. \tag{4.29}$$

Therefore, the attenuation slope can be calculated as

$$\alpha_o = -\frac{1}{4\tilde{\sigma}_c^2}\frac{\partial \tilde{f}_c'}{\partial z_o}. \tag{4.30}$$

Selection of f_c and $\tilde{\sigma}_c$ for Hybrid Method: f_c is often chosen as the frequency where the spectral peak of $GRS(f, z_o)$ is approximately in the middle of the usable frequency range. Similarly, $\tilde{\sigma}_c$ is chosen as the bandwidth of the received echoes from the ROI.

4.3.5 Comparison of Spectral Difference, Spectral Log-Difference, and Hybrid Methods for Local Attenuation Estimation

Before concluding our discussion of local attenuation estimation, we will briefly compare the performance of the three algorithms that utilize a reference phantom as was originally reported in Labyed and Bigelow (2011). These algorithms were selected for comparison because they are the easiest to implement when using modern ultrasound clinical array transducers. We use computer simulations to evaluate the dependence of the algorithms on the number of independent echoes and the number of pulse lengths utilized to obtain the estimates. The simulations utilized a 10 MHz source with a 5 cm focal length and a 50 % −3-dB bandwidth. We assume that the local attenuation has the form $\alpha_{loc}(f) = \alpha_0 f$. Figure 4.6 shows the variance of the estimates as a function of ROI size.

From this figure, it is clear that for any given ROI size, the spectral-difference method has the lowest variance. However, the spectral-difference method is also significantly impacted by any heterogeneities in the tissue (Kim and Varghese 2008; Labyed and Bigelow 2011). The spectral-log difference method and the hybrid method have comparable performance both in terms of variance (Fig. 4.6) and in terms of their robustness to tissue heterogeneity (Labyed and Bigelow 2011). Neither the spectral log-difference nor the hybrid method are impacted by changes in acoustic concentration within the ROI. However, a bias will be introduced when there is a change in the frequency dependence of the scattering. If we assume that the change in frequency dependence results from a variation in the effective scatterer diameter, then the bias is approximately given by

$$Error(Np/cm - MHz) \cong \frac{16.32\, f_{mid}\left(a_{eff}^2(z_p) - a_{eff}^2(z_d)\right)}{c^2\left(z_p - z_d\right)} \tag{4.31}$$

where f_{mid} is the middle frequency of the usable frequency range.

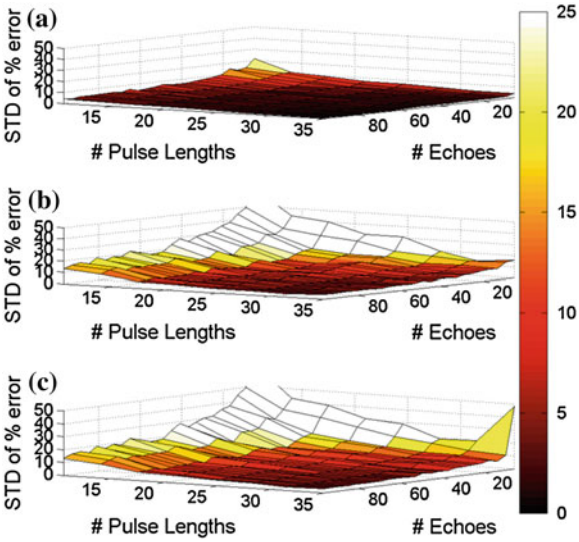

Fig. 4.6 The standard deviation (STD) in the percent error of the attenuation coefficient estimates that were obtained using the spectral difference method from the homogeneous sample, versus the number of pulse lengths and the number of echoes per ROI for the (**a**) spectral difference algorithm, (**b**) the spectral-log difference algorithm, and (**c**) the hybrid algorithm

4.4 Total Attenuation Estimation Algorithms

When performing ultrasound tissue characterization, it is critically important to correct for the frequency dependence of the attenuation along the propagation path. Therefore, in this section we will summarize the two types of algorithms that have been proposed for this purpose. Both of these algorithms assume that the **total attenuation for the sample has a linear frequency dependence** give by $\alpha_{tot}(f) = \alpha_s f$. A third approach, which will not be discussed in detail, would be to use estimates of local attenuation in each of the intervening tissue layers and then sum the estimates to calculate the total attenuation from Eq. (4.2) directly. While this third approach works for some applications with clearly identifiable and relatively thick layers, it tends to have problems when the intervening tissue layers are more complex.

4.4.1 Multiple Filter Algorithm for Total Attenuation Estimation

The first type of algorithm that will be discussed is the multiple-filter algorithm. This algorithm requires either applying multiple Gaussian filters to the backscattered waveforms or using multiple transmit frequencies that span the bandwidth of the transducer (Bigelow 2008, 2010a, b; Labyed and Bigelow 2010). Because most modern tissue characterization applications utilize a clinical array transducer, we will focus our discussion on the use of multiple filters. We use echoes from a reference phantom to correct for diffraction effects.

The algorithm begins with finding the power spectra from a single windowed region in the tissue sample and from the corresponding region in a well-characterized reference phantom. After correcting for the attenuation in the reference phantom, the ratio of the spectra is given by

$$\frac{S_s(f)}{S_{ref}(f)} e^{-\alpha_{ref}(f) z_T} \propto \exp(-4\alpha_s f z_T) \frac{F_\gamma(f)}{F_{\gamma\_ref}(f)} \tag{4.32}$$

where we can assume that the window is located at $z_o = 0$ without loss of generality. We then assume that the frequency dependence of the scattering is approximately given by $F_\gamma(f) \propto \exp(-Af^n)$ where n is approximately equal to 2. While this is clearly true for the Gaussian form factor, it is also true over a limited ka_{eff} range for other common form factors as shown in Fig. 4.7 taken from Bigelow (2010a, b).

In this figure, the fits for each form factor are given by

$$\begin{aligned} F_{\gamma\_Sphere}\left(f,\ a_{eff}\right) &\cong \exp\left(-1.11\left(ka_{eff}\right)^{2.167}\right) \\ F_{\gamma\_Shell}\left(f,\ a_{eff}\right) &\cong \exp\left(-2\left(ka_{eff}\right)^{1.914}\right), \end{aligned} \tag{4.33}$$

and the fit was performed for ka_{eff} from 0 to 1.2 because ka_{eff} values less than 1.2 are of the greatest interest when quantifying the tissue microstructure.

If we then multiply Eq. (4.32) by a series of Gaussian filters, we can show that

$$\frac{S_s(f)}{S_{ref}(f)} e^{-\alpha_{ref}(f) z_T} \exp\left(-\frac{(f-f_c)^2}{2\sigma_c^2}\right) \cong C_1 \exp\left(-\frac{\left(f-\tilde{f}_c\right)^2}{2\sigma_c^2}\right) \tag{4.34}$$

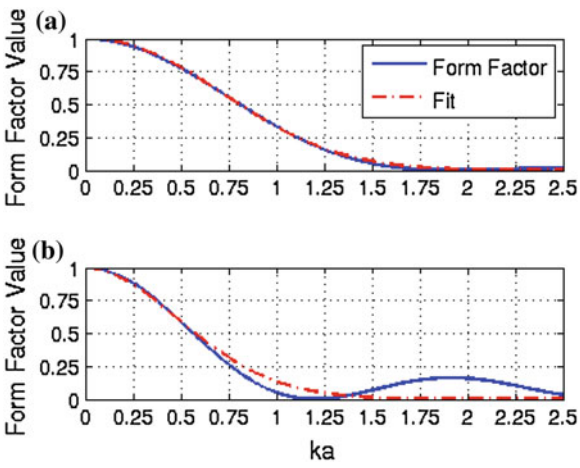

Fig. 4.7 Form factor with fit of the form $\exp(-Af^n)$ for (**a**) fluid filled sphere and (**b**) spherical shell taken from Bigelow (2010a, b)

where

$$\begin{aligned}\tilde{f}_c &\cong \left[1 - 2\tilde{\sigma}_c^2(A_s - A_r)\right] f_c + 4\tilde{\sigma}_c^2 z_T \alpha_s \\ \tilde{\sigma}_c^2 &= \frac{\sigma_c^2}{1 - 2\sigma_c^2(A_s - A_r)}\end{aligned} \tag{4.35}$$

using a derivation similar to that performed for the hybrid method discussed previously. Therefore, for each filter applied, we can find

$$\xi(f_c) = \frac{\left(f_c - \tilde{f}_c\right)}{4\tilde{\sigma}_c^2 z_T} \cong \frac{(A_s - A_r)}{2z_T} f_c - \alpha_s. \tag{4.36}$$

The intercept of $\xi(f_c)$ with respect to f_c will give the slope of the frequency dependence for the total attenuation.

One of the challenges when using the multiple-filter method is determining the optimal number of filters. In an early work, the use of four filters was examined (Bigelow 2010a, b; Labyed and Bigelow 2010). For the first three filters, the center frequency of each filter was calculated as

$$\begin{aligned}f_{c1} &= f_{\min} + \frac{f_{\max} - f_{\min}}{4} \\ f_{c2} &= f_{c1} + \frac{f_{\max} - f_{\min}}{4} \\ f_{c3} &= f_{c2} + \frac{f_{\max} - f_{\min}}{4}\end{aligned} \tag{4.37}$$

where f_{min} and f_{max} were the smallest and largest frequencies of the usable frequency range, respectively. The usable frequency range is the range of frequencies in the power spectrum for which the power spectrum exceeds some level (for example −20 dB) based on the noise level of the received echoes. Once these center frequencies were set, the bandwidths were determined by finding the percent bandwidth such that f_{min} corresponded to the −10 to −15 dB bandwidth for the filter as calculated from

$$\sigma_{c1}^2 = \left(\frac{10(f_{c1} - f_{\min})^2}{2\ln(10)(-BW_{dB})}\right) \tag{4.38}$$

where BW_{dB} is the desired bandwidth (i.e. −10 or −15 dB) for the first filter that would correspond with f_{min}. The bandwidths of the other three filters were then selected to have the same −3-dB percent bandwidth as the first filter. The remaining 4th filter was then selected to span the entire usable frequency range of the backscattered echoes.

Recently, a statistical analysis study was performed on the multiple-filter algorithm to derive an expression for the standard deviation of the total attenuation estimate as a function of ROI size, bandwidth, and number of Gaussian filters (Labyed 2010). The focus was on the variance of the estimates as this is the

limiting criterion when estimating the total attenuation (Bigelow and O'Brien 2005a, b; Bigelow et al. 2005; Bigelow 2008, 2010a, b; Labyed and Bigelow 2010). While it is trivial to get the attenuation correct on average, it is much more challenging to obtain precise estimates especially when the ROI is small. The statistical analysis used non-overlapping (independent) filters to simplify the mathematics and found that the variance in the total attenuation estimate was proportional to

$$\mathrm{var}(\alpha_s) \propto \frac{(N_s + N_r)}{N_s N_r} \frac{1}{\left\{\sum_{j=1}^{K}\left[\sum_{i=1}^{M}(f_i - f_c(j))^2\right]\right\} - \frac{\left\{\sum_{j=1}^{K}\left[\sum_{i=1}^{M}(f_i - f_c(j))^2\right] f_c(j)\right\}^2}{\sum_{j=1}^{K}\left\{\left[\sum_{i=1}^{M}(f_i - f_c(j))^2\right] f_c(j)^2\right\}}} \quad (4.39)$$

where f_i are the individual frequency components of the spectrum, $f_c(j)$ is the center frequency of the jth Gaussian filter when a total of K filters are used, and N_s and N_r are the number of independent echoes used to estimate the power spectra of the sample and reference, respectively.

Precision of Total Attenuation Estimation Algorithms: The precision of the total attenuation estimation algorithms is strongly influenced by the bandwidth of the source and the number of independent echoes used to obtain the estimate. There is also some dependence on the size of the windowed region used to estimate the power spectrum as this can influence the accuracy of the power spectra estimate.

The results of the statistical analysis also revealed that the optimal number of non-overlapping filters is equal to two. In addition, the standard deviation of the total attenuation estimate decreases with increasing ROI size, i.e., with increasing number of independent echo lines used to compute the power spectra, and increasing time window length used to gate the echo lines. Note that the total attenuation is estimated from the power spectrum that is obtained by averaging the power spectra of the windows within the ROI. Therefore, using a large number of echo lines improves the estimate of the power spectrum, and hence improves the estimate of the total attenuation.

The results of the statistical analysis were validated using numerical simulations. Backscattered signals were simulated for a sample and a reference that had attenuation coefficients of 0.7 and 0.5 dB/cm-MHz, respectively. The sample scatterers had a Gaussian Form Factor with a 20 μm effective radius, while the reference had spherical shell scatterers with 10 μm radii. Both the sample and the reference had a scattering density of 100 mm^{-3}, corresponding to approximately 10 scatterers per resolution cell, which is adequate for fully developed speckle.

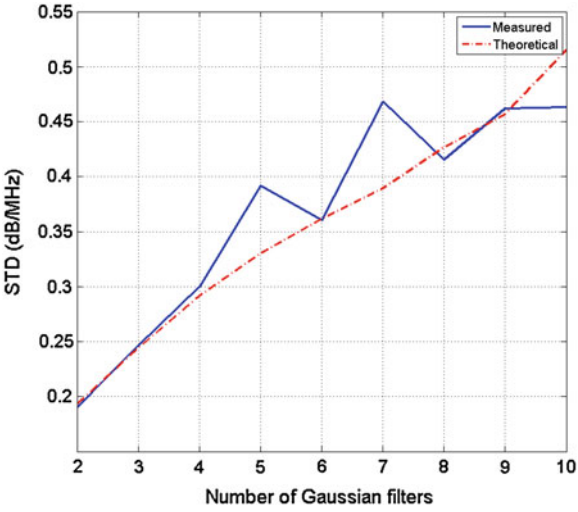

Fig. 4.8 Plots of the theoretical and calculated standard deviation of the total attenuation estimate from the simulated backscattered signals, obtained with the multiple-filter method using an ROI length of 10 pulse lengths and an ROI width of 60 independent echo lines, with respect to the number of non-overlapping filters

Figure 4.8 shows plots of the theoretical and calculated standard deviation of the total attenuation estimate from the simulated backscattered signals as a function of the number of non-overlapping filters. It is clear that using two independent Gaussian filters yields the smallest standard deviation in the estimate of the total attenuation. As shown in Fig. 4.9, the STD in the total attenuation estimate decreased with increasing number of independent echoes.

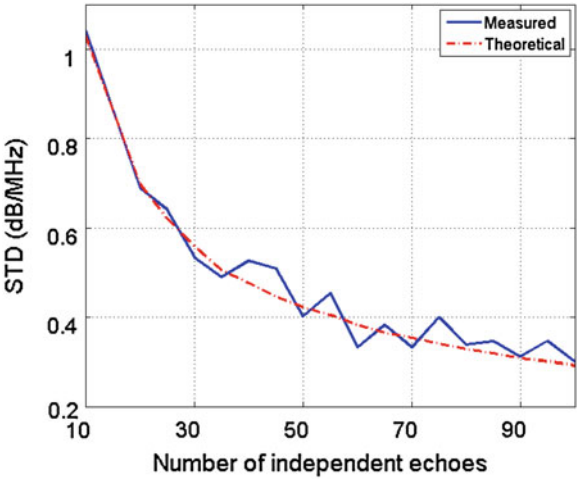

Fig. 4.9 Plots of the theoretical and calculated standard deviation of the total attenuation estimate from the simulated backscattered signals, obtained using the multiple filter method with two Gaussian filters and an ROI length (time window size) of 10 pulse lengths with respect to the number of independent of echoes per ROI

4.4.2 Spectral Fit Algorithm for Total Attenuation Estimation

The second type of algorithm used for obtaining the frequency-dependent attenuation along the propagation path involves estimating the frequency dependence of the backscatter and the attenuation simultaneously. Initially, the tissue was assumed to satisfy a Gaussian form factor $\left(F_{\gamma\_Gaussian}\left(f,\ a_{eff}\right) = \exp\left(-0.827\left(k \cdot a_{eff}\right)\right)\right)$ and a fit was performed to estimate both α_s and a_{eff} (Bigelow and O'Brien 2005a, b; Bigelow et al. 2005). Other authors have extended the algorithm to allow for a more general form for the backscatter $(BSC(f) = bf^n)$ and then perform a fit for b, n, and α_s (Nam et al. 2011). However, we will focus on the original spectral fit algorithm where only two parameters were estimated.

The spectral fit algorithm begins by dividing the spectra from the windowed region of the sample by the spectra from the windowed region of a known reference. Initially, a planar target was used as a reference, but a reference phantom has also been used. Our derivation here will assume a reference phantom is used. After dividing the spectra, the result is multiplied by the attenuation and backscatter terms for the reference as given by

$$S_{fit}(f) = \frac{S_s(f)}{S_{ref}(f)} e^{-\alpha_{ref}(f) z_T} BSC_{ref}(f) \propto \exp(-4\alpha_s f z_T) F_\gamma(f). \tag{4.40}$$

Assuming a Gaussian form factor for $F_\gamma(f)$, the natural log of Eq. (4.40) will yield

$$-\ln\left(S_{fit}(f)\right) = 0.827\left(\frac{2\pi}{c} a_{eff}\right)^2 f^2 + 4\alpha_s f z_T + Constant \tag{4.41}$$

where a simple polynomial fit will yield both the total attenuation slope, α_s, and the effective scatterer radius, a_{eff}.

When implementing the spectral fit algorithm, more accurate and precise estimates are obtained as the frequency range ($\Delta f = f_{max} - f_{min}$) used to obtain the attenuation estimate increases, similar to the case for the multiple filter method (Labyed 2010). Figure 4.10 shows average error and the deviation as a function of frequency range for attenuation values of 0, 0.3, 0.5, and 1 dB/cm-MHz with a_{eff} of 5–105, 5–75, 5–85, and 5–150 μm, respectively taken from Bigelow and O'Brien (2005a, b). Also, shown are the results for a 25 μm a_{eff} and attenuation values varying from 0 to 1 dB/cm-MHz. The results were obtained using a 3 mm Hamming window (~13.5 pulse lengths) and 25 independent echoes. Regardless of the scattering and attenuation properties of the sample, a consistent variance is achieved provided the same Δf is used to obtain the estimates. Figure 4.10 also reiterates that when finding the total attenuation, achieving good accuracy is much easier than achieving small variance.

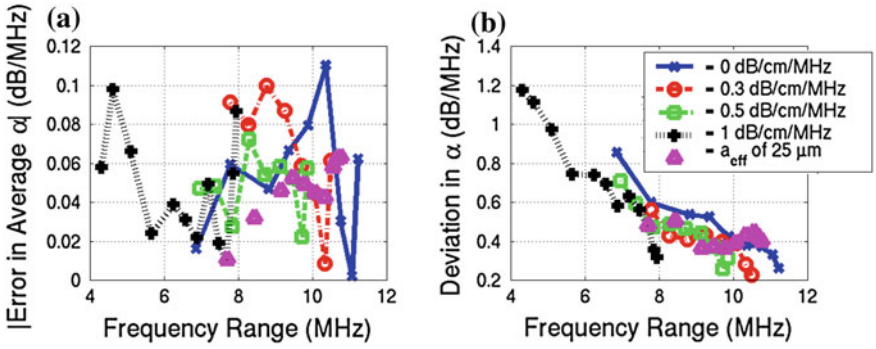

Fig. 4.10 Plots of the **a** accuracy and **b** precison for a range of attenuations and scatterer sizes taken from Bigelow and O'Brien (2005a, b) estimated from simulated backscattered signals illustrating the importance of the frequency bandwidth when estimating the total attenuation using the spectral fit algorithm

Methods to Improve Usable Frequency Range: Because the total attenuation estimation algorithms are highly dependent on bandwidth. One way of increasing the bandwidth is to use higher frequency transducers. Using higher frequency transducers however, limits the penetration depth into tissue. Recently, methods that are based on coded excitation and pulse compression have been shown to improve the bandwidth and penetration depth (Oelze 2007). Surface micro-machined capacitive ultrasonic transducers are new designs that demonstrated a big improvement in the bandwidth (Ladabaum et al. 1998; Ergun et al. 2003). Some ultrasound clinical systems, however, allow the transducer to be excited at three different center frequencies. This feature can be used to increase the usable frequency range in the power spectrum of the backscattered signal.

4.4.3 Comparison of Spectral Fit Algorithm and Multiple Filter Algorithm

As described in Sect. 4.4.1, the optimal number of filters for the multiple-filter method is two. However, that result was only valid when the Gaussian filters were non-overlapping. Therefore, it is important to test whether using overlapping filters can improve the attenuation estimates. A comparison of the performance between the multiple-filter method and the spectral-fit method is also important to consider.

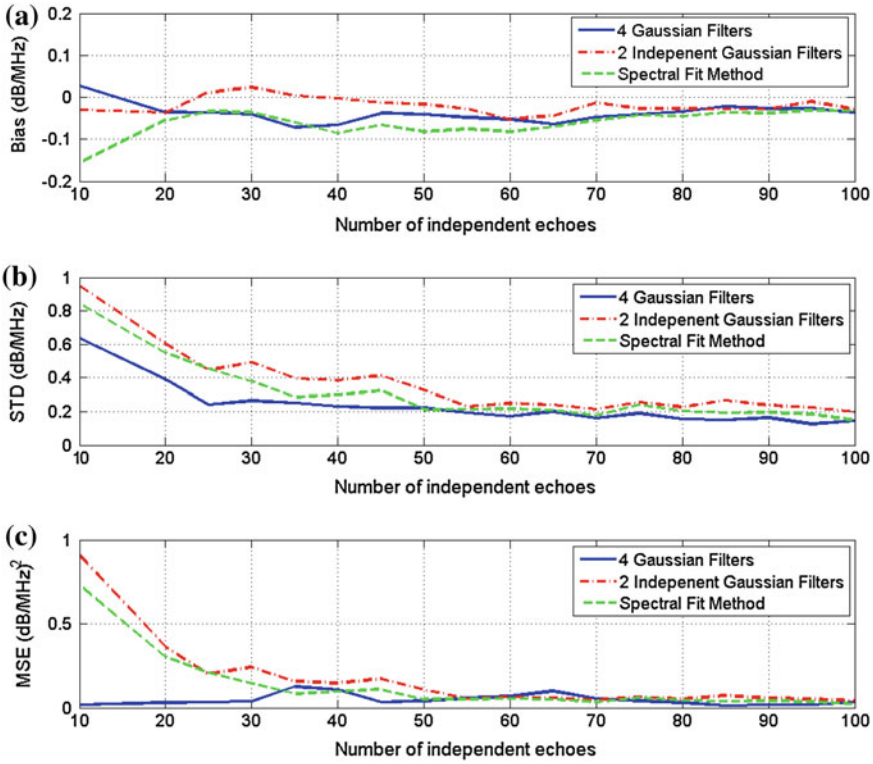

Fig. 4.11 Plots of the **a** bias, **b** STD, and **c** MSE of the estimate α_s, which was obtained using the multiple filter method with two independent Gaussian filters, the multiple filter method with four overlapping Gaussian filters, and the spectral-fit method, with respect to the number of independent of echoes per ROI for an ROI length of 10 pulse lengths

In this section, we compare the bias, STD, and mean squared error (MSE) of the total attenuation estimates obtained with the spectral-fit method, the multiple-filter method that uses two non-overlapping filters, and the multiple-filter method that uses four overlapping filters as described in (see Sect. 4.4.1). We use the numerical simulations described in Sect. 4.4.1 to perform these tests. Figure 4.11 shows the results as a function of number of independent echoes in the sample while Fig. 4.12 gives the results as a function of number of pulse lengths used to estimate the backscattered power spectrum. The results indicate that the variance strongly depends on the number of echoes with only a weak dependence on the number of pulse lengths. However, a slight bias is introduced for smaller pulse lengths that is not observed when the number of independent echoes tends towards zero.

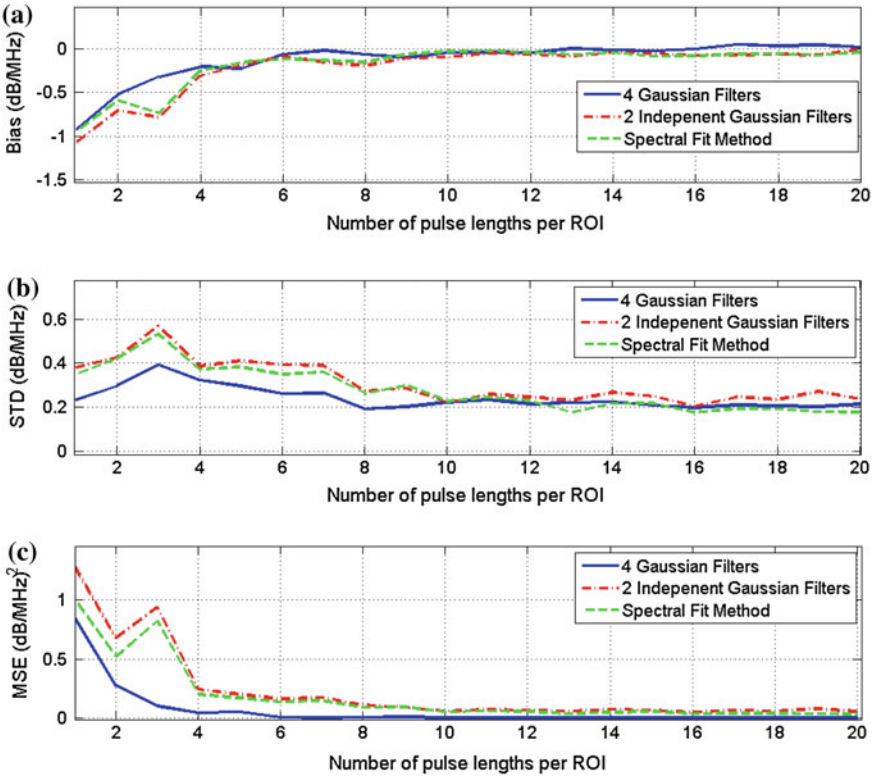

Fig. 4.12 Plots of the **a** bias, **b** STD, and **c** MSE of the estimate α_s, which was obtained using the multiple filter method with two independent Gaussian filters, the multiple filter method with four overlapping Gaussian filters, and the spectral-fit method, with respect the number of pulse lengths per ROI for an ROI that has 50 independent echo lines

ROI Size needed for Total Attenuation Algorithms: A good rule of thumb is to have a windowed region of at least 10 pulse lengths and at least 25 to 35 independent echoes. However, these values are also dependent on the frequency range available for obtaining the estimates.

Based on the two figures below, the MSE is comparable for both the spectral fit method and the multiple filter method with two independent Gaussian filters. However, the spectral fit method provides a slightly smaller STD and a slightly larger bias compared to the two independent filter method. The figures also show in the multiple filter method, that using three overlapping Gaussian filters and a fourth filter that spans the entire usable frequency range gives better results than using only two independent Gaussian filters. This latter result demonstrates that

the multiple filter method could potentially be improved to yield smaller errors in the attenuation estimates by using two overlapping filters.

References

Baldeweck T, Laugier P et al (1993) Application of autoregressive spectral analysis for ultrasound attenuation: interest in highly attenuating medium

Baldeweck T, Herment A et al (1994) Attenuation estimation in highly attenuating media using high frequencies: a comparison study between different mean frequency estimators

Baldeweck T, Laugier P et al (1995) Application of autoregressive spectral analysis for ultrasound attenuation estimation: interest in highly attenuating medium. IEEE Trans Ultrason Ferroelectr Freq Control 42(1):99–110

Barber FE (1991) The scanning acoustic microprobe: I. Analysis and synthesis of a spherically symmetric point spread function. J Acoust Soc Am 90(1):1–10

Bigelow TA (2004) Estimating the medical ultrasound in vivo power spectrum. PhD, Electrical Engineering. University of Illinois, Urbana, p 243

Bigelow TA (2008) Ultrasound attenuation estimation using backscattered echoes from multiple sources. J Acoust Soc Am 124(2):1367–1373

Bigelow TA (2010a) Estimating the total ultrasound attenuation along the propagation path by applying multiple filters to backscattered echoes from a single spherically focused source. IEEE Trans Ultrason Ferroelectr Freq Control 57(4):900–907

Bigelow TA (2010b) Improved algorithm for estimation of attenuation along propagation path using backscattered echoes from multiple sources. Ultrasonics 50(4–5):496–501

Bigelow TA, O'Brien WD Jr (2004a) Scatterer size estimation in pulse-echo ultrasound using focused sources: calibration measurements and phantom experiments. J Acoust Soc Am 116(1):594–602

Bigelow TA, O'Brien WD Jr (2004b) Scatterer size estimation in pulse-echo ultrasound using focused sources: theoretical approximations and simulation analysis. J Acoust Soc Am 116(1):578–593

Bigelow TA, O'Brien WD Jr (2005a) Evaluation of the spectral fit algorithm as functions of frequency range and Dka_{eff}. IEEE Trans Ultrason Ferroelectr Freq Control 52(11):2003–2010

Bigelow TA, O'Brien WD Jr (2005b) Signal processing strategies that improve performance and understanding of the quantitative ultrasound SPECTRAL FIT algorithm. J Acoust Soc Am 118(3):1808–1819

Bigelow TA, O'Brien WD Jr (2006) Impact of local attenuation approximations when estimating correlation length from backscattered ultrasound echoes. J Acoust Soc Am 120(1):546–553

Bigelow TA, Oelze ML et al (2005) Estimation of total attenuation and scatterer size from backscattered ultrasound waveforms. J Acoust Soc Am 117(3):1431–1439

Bigelow TA, McFarlin BL et al (2008) In vivo ultrasonic attenuation slope estimates for detecting cervical ripening in rats: preliminary results. J Acoust Soc Am 123(3):1794–1800

Ergun AS, Yaralioglu GG et al (2003) Capacitive micro machined ultrasonic transducers: theory and technology. J Aerosp Eng 16(2):76–84

Girault JM, Ossant F et al (1998) Time-varying autoregressive spectral estimation for ultrasound attenuation in tissue characterization. IEEE Trans Ultrason Ferroelectr Freq Control 45(3):650–659

Insana M, Zagzebski J et al (1983) Improvements in the spectral difference method for measuring ultrasonic attenuation. Ultrason Imaging 5(4):331–345

Insana MF, Wagner RF et al (1990) Describing small-scale structure in random media using pulse-echo ultrasound. J Acoust Soc Am 87(1):179–192

Kim H, Varghese T (2007) Attenuation estimation using spectral cross-correlation. IEEE Trans Ultrason Ferroelectr Freq Control 54(3):510–519

Kim H, Varghese T (2008) Hybrid spectral domain method for attenuation slope estimation. Ultrasound Med Biol 34(11):1808–1819

Kuc R (1980) Clinical application of an ultrasound attenuation coefficient estimation technique for liver pathology characterization. IEEE Trans Biomed Eng BME 27(6):312–319

Kuc R (1984) Estimating acoustic attenuation from reflected ultrasound signals: comparison of spectral-shift and spectral-difference approaches. IEEE Trans Acoust Speech Signal Process 32(1):1–6

Kuc R, Schwartz M (1979) Estimating the acoustic attenuation coefficient slope for liver from reflected ultrasound signals. IEEE Trans Sonics Ultrason 26(5):353–361

Labyed Y (2010) Optimization and application of ultrasound attenuation estimation algorithms. PhD Electrical and computer engineering. Iowa State University, Ames, 179

Labyed Y, Bigelow TA (2010) Estimating the total ultrasound attenuation along the propagation path by using a reference phantom. J Acoust Soc Am 128(5):3232–3238

Labyed Y, Bigelow TA (2011) A theoretical comparison of attenuation measurement techniques from backscattered ultrasound echoes. J Acoust Soc Am 129(4):2316–2324

Ladabaum I, Xuecheng J et al (1998) Surface micromachined capacitive ultrasonic transducers. IEEE Trans Ultrason Ferroelectr Freq Control 45(3):678–690

Nam K, Zagzebski JA et al (2011) Simultaneous backscatter and attenuation estimation using a least squares method with constraints. Ultrasound Med Biol 37(12):2096–2104

Narayana PA, Ophir J (1983a) A closed form method for the measurement of attenuation in nonlinearly dispersive media. Ultrason Imaging 5:17–21

Narayana PA, Ophir J (1983b) On the validity of the linear approximation in the parametric measurement of attenuation in tissues. Ultrasound Med Biol 9(4):357–361

Oelze ML (2007) Bandwidth and resolution enhancement through pulse compression. IEEE Trans Ultrason Ferroelectr Freq Control 54(4):768–781

Oelze ML, O'Brien WD Jr (2002) Frequency-dependent attenuation-compensation functions for ultrasonic signals backscattered from random media. J Acoust Soc Am 111(5):2308–2319

Oelze ML, O'Brien WD Jr (2006) Application of three scattering models to characterization of solid tumors in mice. Ultrason Imaging 28(2):83–96

Oosterveld BJ, Thijssen JM et al (1991) Ultrasound attenuation and texture analysis of diffuse liver disease: methods and preliminary results. Phys Med Biol 36(8):1039–1064

Parker KJ, Waag RC (1983) Measurement of ultrasonic attenuation within regions selected from B-Scan images. IEEE Trans Biomed Eng BME 30(8):431–437

Parker KJ, Lerner RM et al (1988) Comparison of techniques for in vivo attenuation measurements. IEEE Trans Biomed Eng 35(12):1064–1068

Yao LX, Zagzebski JA et al (1990) Backscatter coefficient measurements using a reference phantom to extract depth-dependent instrumentation factors. Ultrason Imaging 12(1):58–70